Mountain Torque Events at the Tibetan Plateau

JOSEPH EGGER

Meteorologisches Institut der Universität München, Munich, Germany

KLAUS-PETER HOINKA

DLR, Oberpfaffenhofen, Germany

(Manuscript received 19 December 2006, in final form 26 April 2007)

ABSTRACT

The interaction of large-scale wave systems with the Tibetan Plateau (TP) is investigated by regressing pressure, potential temperature, winds, precipitation, and selected fluxes in winter onto the three components T_{oi} of this massif's mountain torque on the basis of the 40-yr ECMWF reanalysis (ERA-40) data. Events with respect to the equatorial "Greenwich" axis of the global angular momentum exhibit by far the largest torques ($T_{o1,}$), which essentially represent north–south pressure differences across the TP. The axial torque T_{o3} peaks when the surface pressure is high at the eastern slope of the TP. The torque T_{o2} with respect to the 90°E axis is closely related to T_{o3} with $T_{o2} \sim -T_{o3}$. The maximum (minimum) of T_{o1} tends to occur about 1 day earlier than the minimum (maximum) of T_{o2}. All torque events are initiated by equivalent barotropic perturbations moving eastward along the northern rim of the TP. In general, the initial depression, for example, forms a southward-protruding extension at the eastern slope of the TP and a new high grows near Japan. Later, the perturbation near Japan moves eastward in T_{o2} events but extends northward in T_{o1} events. These flow developments cannot be explained by theories of topographic instability. The observed vertical motion at the lee slope is at best partly consistent with theories of linear quasigeostrophic wave motion along mountain slopes. These findings lead the authors to test the eventual usefulness of linear theories by fitting the linear terms of a novel statistical equation for the potential temperature θ to the observed changes of θ and the torque to the observations. This test indicates that the evolving regression patterns of θ can be explained by linear terms at least in specific domains. In turn, pressure tendency regressions at a selected level can be calculated on the basis of the linear θ tendencies above that level. The formation of the lee trough appears to be mainly caused by horizontal warm-air advection along the slopes, but changes of the potential temperature above the height of the TP also contribute significantly to the pressure changes in the lee. Cold-air advection aloft strengthens the Japan high. "Turbulent" transports appear to be mainly responsible for the decay of the perturbations but data accuracy problems impede the analysis. In particular, the noisiness of the vertical motion fields affects the skill of the linear calculations.

1. Introduction

The impact of the Tibetan Plateau (TP) on baroclinic systems is amply documented by numerous case studies and, to some extent, also by climatological analyses (e.g., Academia Sinica 1958; Joung and Hitchman 1982; Hakim 2003). A wide variety of methods has been applied to this problem. Investigations of cyclone tracks and cyclogenetic frequencies (e.g., Chen et al. 1991; Hoskins and Hodges 2002) clearly reflect the impact of the TP. Additional information can be extracted by relating the observed flow evolution near a mountain to a suitably chosen interaction parameter. Murakami (1981) selected the principal component of an EOF expansion of meridional flows at 200 hPa above the TP as a parameter to find pressure cells moving along the eastern periphery of the TP. Hsu and Wallace (1985) related the surface pressure and 500-hPa height field evolution near the TP to the principal components of an EOF expansion of surface pressure. They found a fairly distinct equatorward propagation of the near-surface patterns "parallel to contours of surface elevation" along the eastern slope of the TP. Chang (2005)

Corresponding author address: Joseph Egger, Meteorologisches Institut der Universität München, Theresienstr. 37, Munich 80333, Germany.
E-mail: j.egger@lrz.uni-muenchen.de

DOI: 10.1175/2007MWR2126.1

applied similar techniques at points downstream of the TP and found that wave trains passing this point in the winter on their way to the east originate either from northern Asia around 60°N or from the subtropical jet region south of the TP.

The axial mountain torque exerted by the TP [see also Eq. (1.1)] reflects the zonal pressure difference across the mountain massif and is, therefore, another useful indicator of the interaction of synoptic systems with this obstacle. For example, Weickmann (2003) regressed the axial torque exerted by the TP onto flow features at 250 hPa and the surface pressure. He found that positive torque events are associated with the eastward propagation of an upper-level trough near the TP and with the anticyclonic motion of surface pressure patterns around the plateau in the east. Lott et al. (2004) conducted a similar investigation but were mainly interested in low-frequency events where this anticyclonic motion is but weakly visible.

It is fair to say that there exists no generally accepted explanation for the observed developments in the lee of the TP. Quasigeostrophic theory provides guidance with respect to the interaction of synoptic-scale perturbations with huge zonally oriented massifs (Buzzi et al. 1987; Davis and Stoelinga 1999). The propagation speed of the waves is affected by the mountain induced changes of the near-surface temperature field. This way, the eastward propagation of baroclinic waves should be accelerated at the TP's northern slope and retarded in the south. Moreover, baroclinic waves may be guided along the slopes (Murakami and Nakamura 1983; Davis 1997). For example, a warm low moving eastward along the northern flank may turn southward at the TP's northeastern corner because the anomalous westerlies at upper levels linked to the low descend above the eastern lee slope and induce a warming there. Pressure fall and southward extension of the low may follow. The theory of topographic instability (Charney and DeVore 1979; Jin and Ghil 1990) involves mountain torques to explain the pressure fall in the lee of the TP. Hakim (2003) invoked the concept of downstream development related to the theory of wave packets in unstable baroclinic flows (e.g., Pierrehumbert and Swanson 1995) to explain observed cyclone growth downstream of the TP. Intercomparison of the theoretical predictions with the evolution of wave packet ensembles turned out to be encouraging. It has to be kept in mind, however, that the evolution of the corresponding correlation maps with lag is at best partly governed by linear deterministic dynamics (Hakim 2003). There is no way to explain the rapid buildup and decay of these correlations without taking the stochastic nature of these processes into account

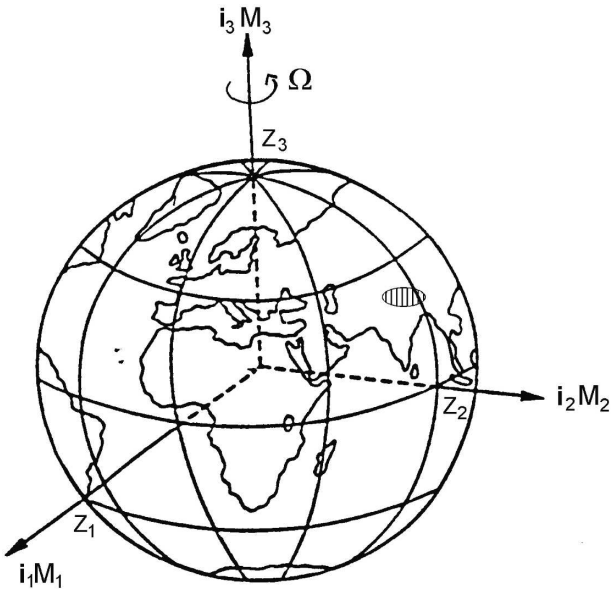

FIG. 1. Rotating earth and the components $\mathbf{i}_i\mathbf{M}_i$ of the global angular momentum. The TP is hatched. Also given are the poles Z_i of the $(\tilde{\lambda}_1, \tilde{\varphi}_i)$ systems adapted to the axes $\mathbf{i}_i$. In particular, Z_1 (Z_2) is the "Greenwich" pole (90°E pole).

[see also Egger and Hoinka (2006, hereinafter EH06) and references therein].

EH06 studied the impact of Greenland on synoptic systems by invoking statistical flow equations that describe the relation of the axial mountain torque and the synoptic development. This approach turned out to be quite useful and will, therefore, be applied here in modified form. We expect that meridional pressure differences across the TP are larger than the zonal ones (see also Chang 2005) and that the corresponding torque events represent somewhat different flow situations. For this reason we include in our analysis the mountain torques with respect to the equatorial components M_1 and M_2 of the global angular momentum $\mathbf{M} = \Sigma_{i=1}^{3} M_i\mathbf{i}_i$ as basic parameters for data stratification. The equatorial component $M_1\mathbf{i}_1$ points toward the Greenwich meridian (Fig. 1) and there is also a 90°E component $M_2\mathbf{i}_2$. The axial component $M_3\mathbf{i}_3$ is, of course, aligned with the earth's rotation axis.

Although the formulas for the equatorial mountain torques are fairly complicated when expressed in standard spherical (λ, φ) coordinates, they become rather simple when a rotated coordinate system $(\tilde{\lambda}_i, \tilde{\varphi}_i, z)$ is introduced for each angular momentum axis where the basic vector $\mathbf{i}_i$ is the "polar" axis, that is, if the point Z_i as given in Fig. 1 is the "North Pole" of this system. The other unit vectors $\mathbf{i}_j$ are then embedded in the "equatorial" plane $\tilde{\varphi}_i = 0$. The mountain torque with respect to this axis is

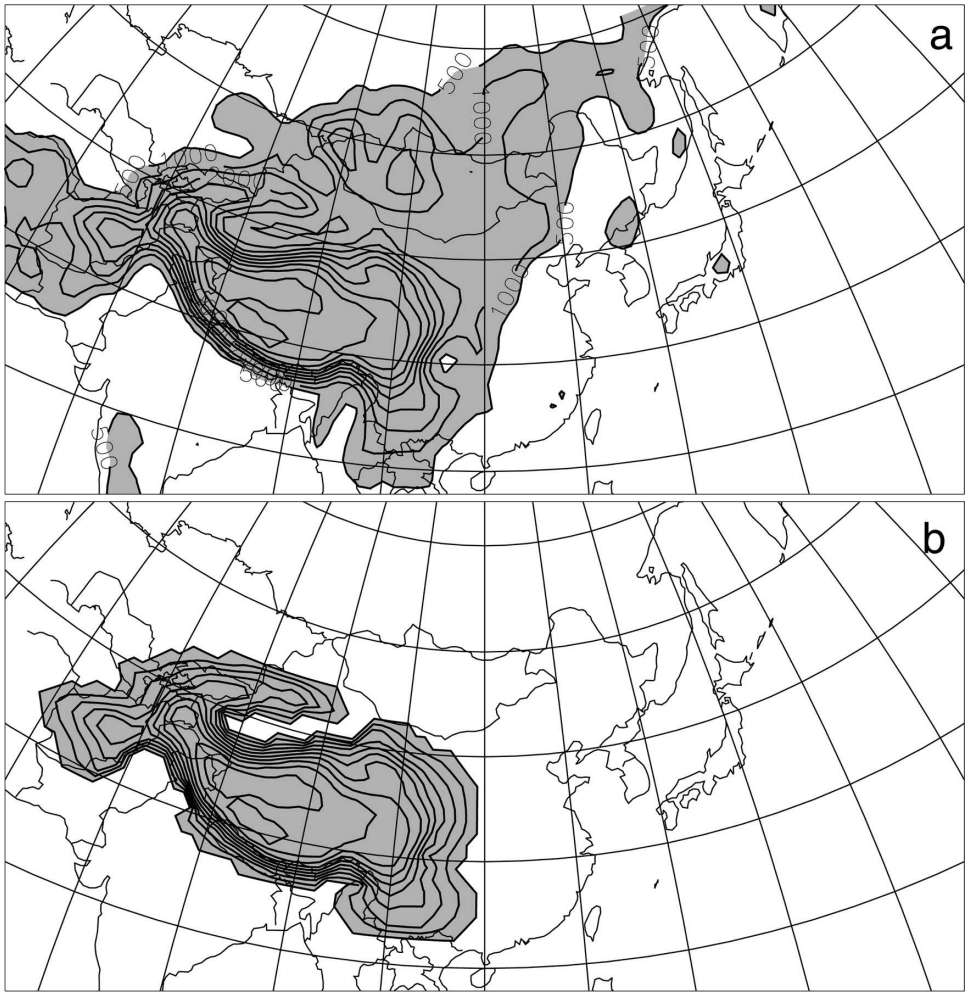

FIG. 2. Topography of the analysis domain as used in (a) the original ERA scheme and (b) the torque calculations. The contour interval is 500 m.

$$T_{\mathrm{oi}} = -\int_F p_s \frac{\partial h}{\partial \tilde{\lambda}_i}\, df, \tag{1.1}$$

where $\tilde{\lambda}_i$ is "longitude," p_s is the surface pressure, h is the topography, and F is a selected area for which the torque is evaluated. The actual calculation of the torques is based on a topographic profile (see Fig. 2b), which differs somewhat from that used in the 40-yr European Centre for Medium-Range Weather Forecasts (ECMWF) reanalysis (ERA-40) (Fig. 2a) in order to have an isolated obstacle (see the appendix for details). The interpretation of (1.1) is simple. Whenever the surface pressure on the upslope side of a mountain is larger than on the downslope side, the atmosphere loses angular momentum with respect to the corresponding axis. "Upslope" means ascent when we follow latitude circles $\tilde{\varphi}_i$ = constant assuming the conventional cyclonic orientation of the coordinate system. This means, in particular, that high pressure to the north of the TP is associated with positive torques $T_{\mathrm{o1}} > 0$ with respect to the Greenwich axis. High pressure to the west of the plateau means positive torques with respect to M_2 and negative ones with respect to M_3. It is obvious that the passage of synoptic systems near the TP generates torques with respect to all the three components of the global angular momentum. It is, however, not clear if all baroclinic systems moving along the TP exert a substantial torque. Note that we use the torques only as convenient stratification parameters. Their impact on the motion of the solid earth will not be discussed.

The winter season December–February (DJF) with its cold air outbreaks is selected for this investigation. The standard deviations of the three torque components are $\sigma_1 = 23$, $\sigma_2 = 6$, and $\sigma_3 = 10$ Hadleys (1 Hadley = 10^{18} J). The dominance of the Greenwich

torques reflects partly the zonal elongation of the TP but the north–south pressure differences across the TP are also larger than those in zonal direction. It is convenient to normalize all torques by their standard deviations σ_i to provide the basic parameters $T_i = T_{oi}/\sigma_i$ onto which the available flow variables are regressed.

The autocorrelations of the torques decay fairly quickly (Fig. 3; see also Weickmann 2003). There is, however, no zero crossing since low-frequency atmospheric variability contributes to the torques. The torques T_i are closely related. The latitude circles $\tilde{\varphi}_1 =$ constant with respect to the Greenwich pole Z_1 are oriented almost at right angles to those with respect to Z_2 in the Himalayan region while those with respect to Z_2 and Z_3 are almost antiparallel. This implies via (1.1) that $T_{o3} \sim -T_{o2}\cos(55°)/\cos(35°) = -0.7T_{o2}$, where the latitudes in this formula simply reflect the fact that the TP is at ~55° latitude with respect to the pole Z_2. The factor 0.7 is close to the ratio $\sigma_3/\sigma_2 \approx 0.6$ of the standard deviations. The correlation coefficient of T_{o2} and T_{o3} is −0.93 and the cross-correlation function is fairly symmetric with respect to $\tau = 0$. It is, therefore, sufficient to concentrate on the equatorial torques T_1 and T_2. Results for T_3 follow from those for T_2 by a change of sign. Similar geometrical considerations suggest that T_{o1} and T_{o2} are negatively correlated. As can be seen from Fig. 3, the correlation attains a minimum of −0.73 for the lag $\tau = 1$ day. This suggests that T_1 and T_2 events will follow a similar path. For example, T_1 is close to its maximum when cold air banks up against the TP. Shortly afterward, this cold air is moving southward in the lee and T_2 approaches a minimum.

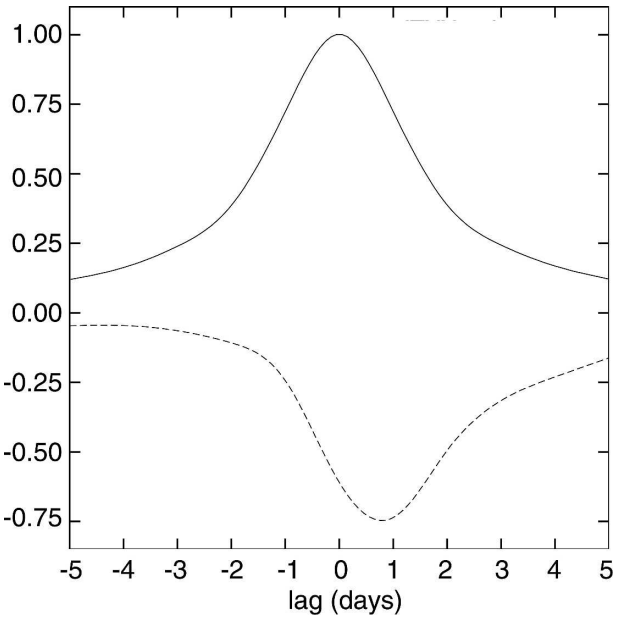

FIG. 3. Autocorrelation of the mountain torque T_{o1} as a function of lag (solid; days) and cross correlation of T_{o1} and T_{o2} (dashed; T_{o1} leading) in winter.

2. Data and methods

The torque regressions are based on data that are part of the ERA-40 dataset covering the period January 1958–December 2001 generated by the ECMWF Reanalysis Project (Uppala et al. 2005). The domain 9°–60.7°N, 49.5°–169.9°E is selected for the analysis. As can be seen from Fig. 4, this domain covers most of the Indian subcontinent, the TP with its foreland to the north, Southeast Asia, and a large part of the Pacific Ocean east of the plateau. All data of the ERA-40 set are transformed such that they are available at the points of a 1.125° × 1.125° grid in the horizontal and at 13 constant height surfaces with a vertical spacing $D_z =$ 1000 m with the lowest level at $z = 500$ m. Daily precipitation is provided at all points of the horizontal grid. All data used in the analysis are averages over the four values available per day.

The covariance functions of pressure p, potential temperature θ, vorticity, and precipitation P with all T_i are evaluated for the winter season at every grid point for all layers (except P) and for lags -5 days $\le \tau \le 5$ days. In addition the flux covariances $C[T_i, (v\theta)|\tau]$ are computed as well, where the covariance of variable b leading variable c with lag τ is denoted by $C(b, c|\tau)$.

The covariance fields describe the course of torque events in time and have to satisfy corresponding statistical equations. Vorticity covariances turned out to be too noisy to be useful in a statistical vorticity equation in contrast to the situation near Greenland (EH06). Instead, we consider the "conservation" equation

$$\rho_o \frac{\partial \theta}{\partial t} + \nabla_3 \cdot (\rho_o \mathbf{v}\theta) = \rho_o S_\theta \tag{2.1}$$

for the potential temperature θ where "deep" incompressibility is assumed with reference density $\rho_o(z)$. The term S_θ represents the diabatic sources and sinks. This equation can be turned into a statistical equation suited to our analysis after introducing the standard separation $c = \bar{c} + c'$ for all variables where the bar represents the time mean. Multiplication of (2.1) by $T_i(t - \tau)$ and the formation of expectations yields after simple manipulations

$$\rho_o \frac{\partial}{\partial \tau} C(T_i, \theta|\tau) = -\rho_o L_\theta - \nabla_3 \cdot \rho_o C(T_i, \mathbf{v}'\theta'|\tau) + C(T_i, S_\theta|\tau), \tag{2.2}$$

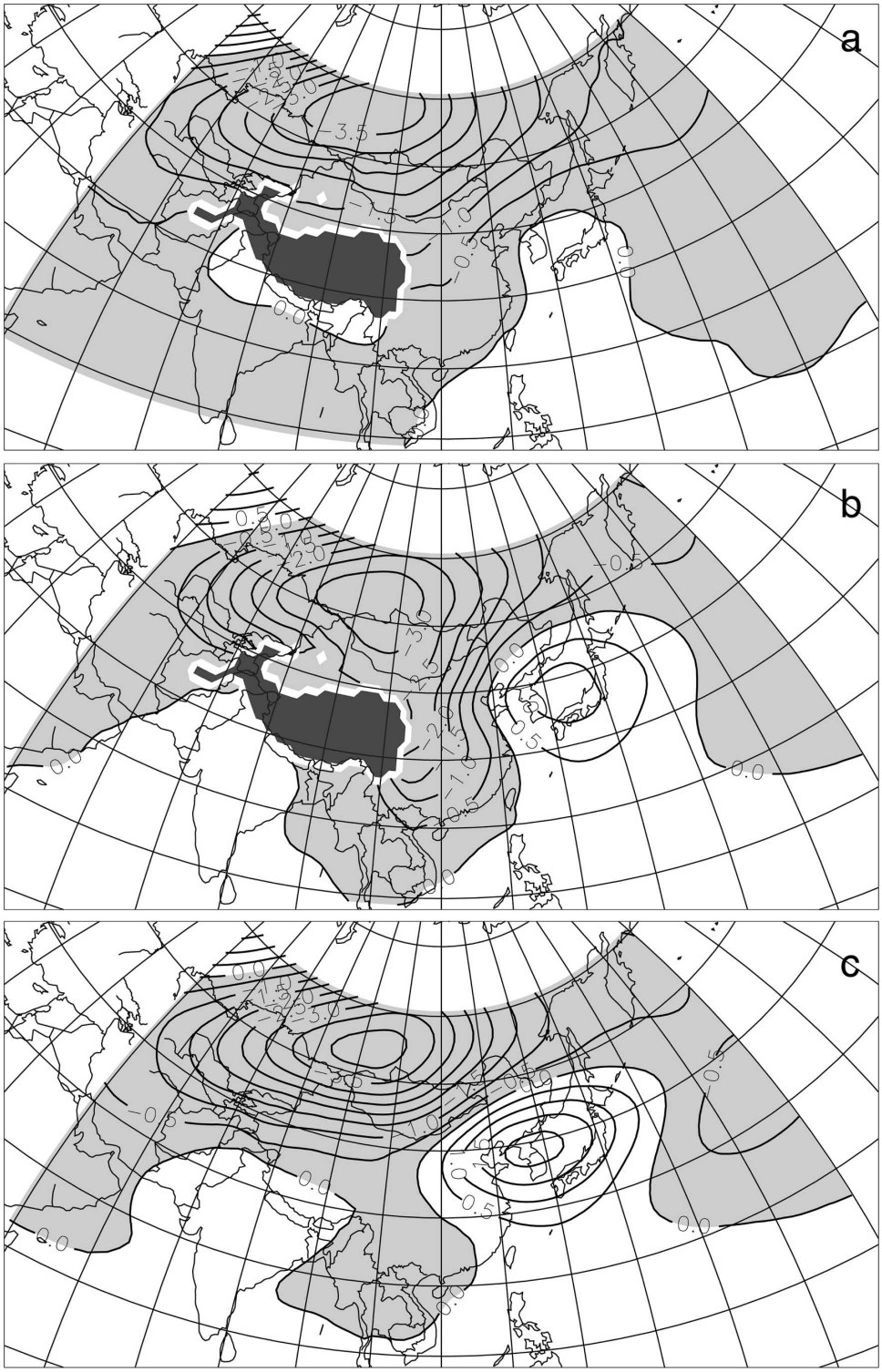

FIG. 4. Covariance $C(T_2, p\,|\,\tau)$ of T_2 with pressure (hPa) in winter at $z = 2500$ m at $\tau =$ (a) -2 and (b) 0 days; (c) $\tau = 0$ days and $z = 5500$ m. The contour interval is 0.5 hPa; negative values are shaded.

where

$$L_\theta = [\overline{\mathbf{v}} \cdot \nabla C(T_i, \theta|\tau) + C(T_i, \mathbf{v}|\tau) \cdot \nabla \overline{\theta}] = L_{2\theta} + L_{3\theta} \tag{2.3}$$

represents the linear terms on the right-hand side of (2.2), which may be split in a horizontal part $L_{2\theta}$ and the contribution $L_{3\theta}$ mainly by vertical motions. If every positive torque event would have an exact negative torque analog, the triple terms in (2.2) would vanish. The triple terms capture typical differences between positive and negative events. They are the "turbulent" fluxes in this problem.

Given the "tendencies" of the θ covariances in (2.2) we are able to calculate also the pressure tendency at some level z_o by integrating the hydrostatic tendency relation:

$$\frac{\partial^2}{\partial\tau\partial z} C(T_i, p|\tau) + g\rho_o c_v \frac{\partial}{\partial\tau} C(T_i, p|\tau)/c_p\overline{p} = g\rho_o \frac{\partial}{\partial\tau} C(T_i, \theta|\tau)/\overline{\theta} \tag{2.4}$$

downward from the top to $z = z_o$. At the top level, we may either assume a vanishing pressure covariance tendency or the observed one. Note, that (2.4) follows from the standard hydrostatic relation by replacing density ρ by potential temperature and by differentiating the resulting relation with respect to time. As yet, neither (2.2) nor (2.4) have been used in climatological analyses. We insert the observed linear covariances L_θ in (2.2) and (2.4) to see to what extent these terms are important in determining the observed tendencies. The forcing terms are not available and the triple terms turned out to be too noisy.

Since only the linear version of (2.2) is available, we have first to test the linearity of the observed changes of potential temperature. This can be done by minimizing the following expression:

$$Z_\theta^2 = \left[\frac{\partial}{\partial\tau} C(T_i, \theta|\tau) + \alpha L_{2\theta} + \beta L_{3\theta}\right]^2 \tag{2.5}$$

for regions Q with $|x - x_o| < D$, $|y - y_o| < D$ centered at the point (x_o, y_o). The coefficients (α, β) in (2.5) are determined by a least squares fit of the sum of all Z_θ^2 evaluated at the M grid points of the region Q. The resulting vector $\mathbf{I} = (\alpha, \beta)$ represents the contribution of the linear terms to the tendency. Perfect linearity is found if $\alpha = \beta = 1$ and if the sum over all Z_θ^2 is small. In that case, there is a chance that a linear theory is helpful in explaining the observed development. If, on the other hand, α and β are close to zero, the linear terms predict too strong changes by far while values $(\alpha, \beta) > 2$, for example, indicate that the contribution by the linear terms is too small. The perfect vector length is $d = (\alpha^2 + \beta^2)^{1/2} = 1.4$. Linear theory is assumed to be of little help when d is outside the range of

$$0.7 \le d \le 2.8. \tag{2.6}$$

Moreover, we require $\alpha > 0$, $\beta > 0$. The minimization of (2.5) involves some smoothing and reduces, therefore, the noisiness inherent in forecasts based on (2.2). This noisiness will turn out to be the main drawback of this method. Even if d is outside the range in (2.6) the failure of the linear approximation may be due to statistical noise generated by the evaluation of the covariances. Linear forecasts may still be possible on the basis of better analyses.

3. Results

As stated above, we restrict the analysis to the equatorial torques in the winter season. It is obvious from (2.2) that the mean flow is quite important in the dynamics of the regression patterns. In winter, the Siberian Mongolia high is the dominant feature of the surface pressure distribution over the continent with corresponding anticyclonic near-surface flow (e.g., Ramage 1971). This high is fairly shallow (Chan and Li 2004). At upper levels, there is high pressure above the TP with the polar jet to the north and the subtropical jet in the south. We will first deal with the T_2 winter case to make sure that the results of Weickmann (2003) are recovered.

a. Equatorial torque T_2 in winter

As mentioned above, Weickmann (2003) found an extended positive surface pressure anomaly to the north of the TP at $\tau = -3$ days, which moves anticyclonically around the massif during the next days. Low pressure prevails above the plateau at $\tau = 3$ days in his analysis of axial torque events. We find quite similar patterns but, of course, with a change of sign. A low is seen at $z = 2500$ m north of the massif at $\tau = -2$ days in Fig. 4a. The zonal diameter of this eastward-moving "parent low" is ~80°–100° longitude. Pressure anomalies are positive near Japan. There is pressure fall all along the eastern slope of the TP and pressure rise in the Pacific (Fig. 4b). We find a pressure difference of ~3 hPa at $\tau = 0$ between the axis of the low pressure tongue and the high near Japan, which was less than 1 hPa two days before (see Fig. 4a). The pressure fall in the lee contributes, of course, to the increase of the torque. The high is beginning to move eastward from $\tau = 2$ days onward while the low north of the TP decays.

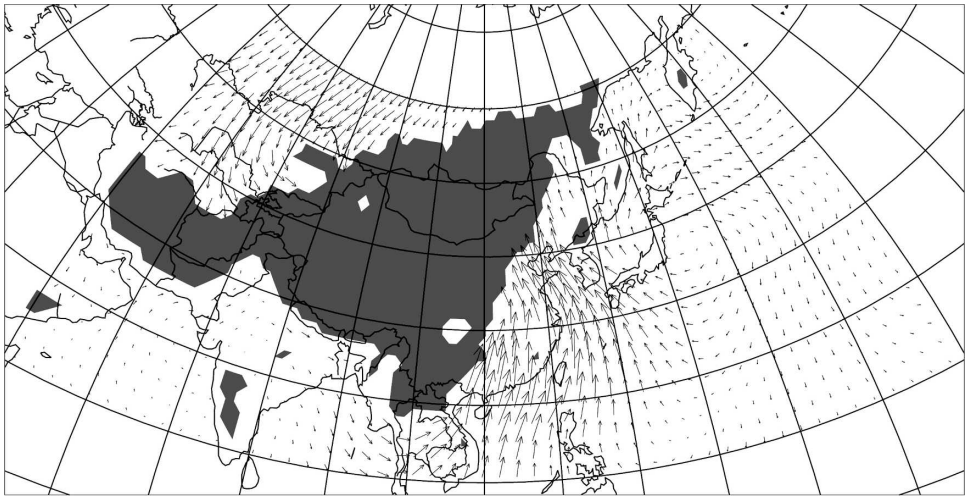

FIG. 5. Covariance $C(T_2, \mathbf{v}_2|\tau)$ of T_2 with the horizontal wind in winter at $z = 500$ m and $\tau = 0$. Maximum wind speed is 3.6 m s^{-1}; dark: topography.

The agreement with Weickmann (2003) is not perfect, of course. For example, the Japan high at $\tau = 0$ in Fig. 4b is stronger than in Fig. 2 of Weickmann (2003). It is clear from Fig. 4 that T_1 and T_2 must be negatively correlated.

The patterns higher up are similar to those at $z = 2500$ m but simpler. At $\tau = -2$ days, there is a zonally elongated trough to the north of the plateau and a belt of weak positive pressure anomalies in the south at $z = 5500$ m (not shown). At $\tau = 0$ days, indications of the "leeside low" are found even at this height, but the new Pacific high and the trough in the north are the dominant features of the pressure distribution (Fig. 4c). The pressure anomalies found at $z = 9500$ m (not shown) correspond quite closely with the findings of Weickmann (2003). The pressure centers move rather slowly at least till $\tau = 3$ days. In particular, the trough north of the TP is almost stationary. There is, however, substantial growth from $\tau = -3$ days till $\tau = 0$.

The axis of the Japan high tilts westward with height at least up to the tropopause, so that we are looking here indeed at baroclinic wave structures. On the other hand, the trough to the north of the TP exhibits little, if any tilt. It is difficult to assign a phase speed to these patterns. The Japan high is fairly stationary at least until $\tau \sim 1$ day, when it is beginning to move eastward. The large scale, the equivalent barotropic structure, and the slow motion of the parent low contrasts with the characteristics of the baroclinic waves found by Chang and Yu (1999), Hakim (2003), and Chang (2005) for that region with wavelengths of ~5000 km, phase speeds of ~10 m s^{-1}, and pronounced vertical tilts. In other words, these waves contribute little to the torque.

The near-surface wind field is cyclonic north of the plateau with an upslope component in the northwest at $\tau = -2$ days, but the flow speeds are small. At $\tau = 0$ days more vivid winds are seen southwest of the TP with maximum speeds of ~4 m s^{-1} (Fig. 5). These relatively strong winds with their upslope component are clearly associated with the low in the lee and the high near Japan.

At $\tau = -4$ days the TP is surrounded by warm air (not shown) but the temperature anomalies are quite small. Amplitudes grow with increasing lag. The warm patch north of the TP moves eastward for $\tau \to 0$ and also extends farther southward with a 2.5-K maximum at the lee slope (Fig. 6a). This warming fits, of course, the pressure fall in the lee in Fig. 4. Three days later, cool air in the rear of the trough dominates the northern part of the analysis domain completely while warm air extends far across the Pacific (Fig. 6b).

The precipitation anomalies for $\tau < 0$ have a maximum in the region of upslope flow northwest of the plateau remnants that can even be seen at $\tau = 2$ days in Fig. 7. There is a patch of positive rainfall anomalies at $\tau = 0$ in the area of upslope flow in Fig. 5. Less rainfall than normal occurs west of the crest. Two days later (Fig. 7), the rainfall pattern has two centers, one near the TP and another one in the area of southerlies associated with the high near Japan (see Fig. 4). The rainfall area at $\tau = 2$ days coincides almost exactly with the domain of positive temperature covariances at that time (see also Fig. 6). There is a rainfall minimum over Myanmar (Burma). The rainfall anomalies near the TP abate till $\tau = 5$ days while the positive precipitation domain in the east is moving slowly eastward. There is

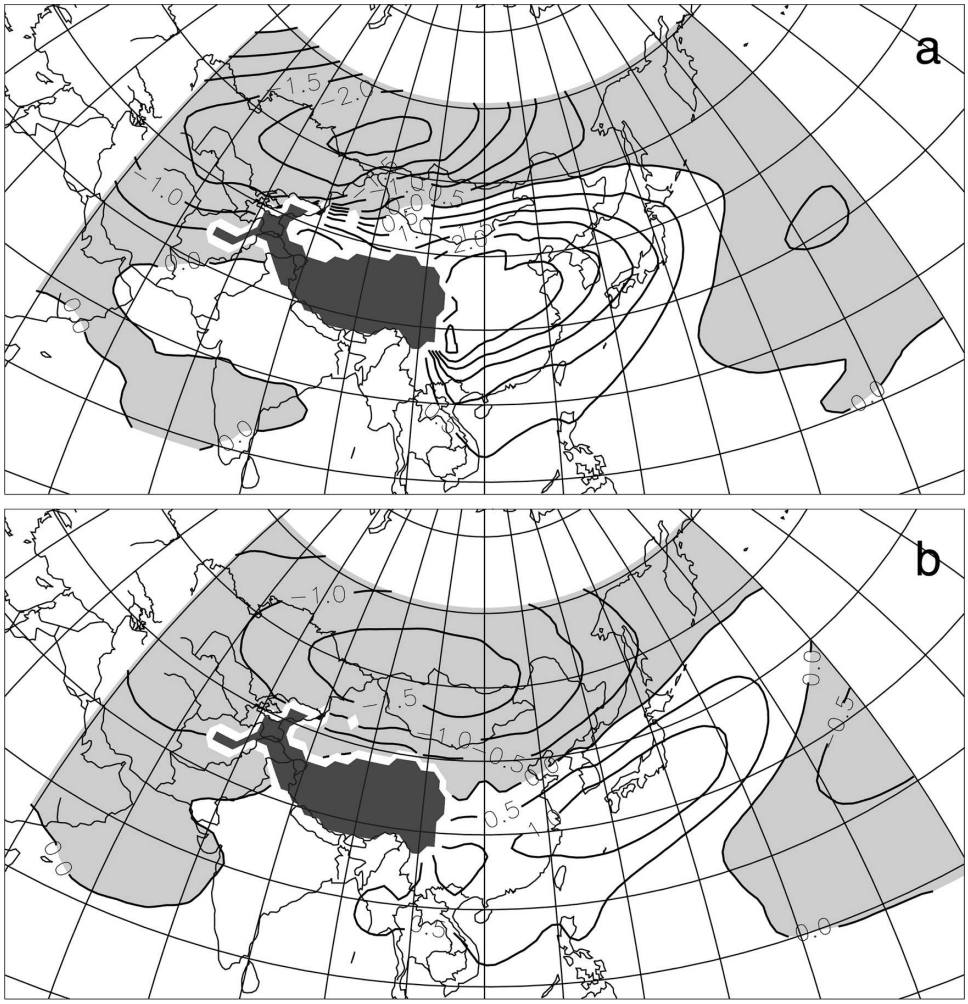

FIG. 6. Covariance $C(T_2, \theta|\tau)$ of T_2 with potential temperature (K) at $z = 2500$ m in winter for (a) $\tau = 0$ and (b) $\tau = 3$ days. The contour interval is 0.5.

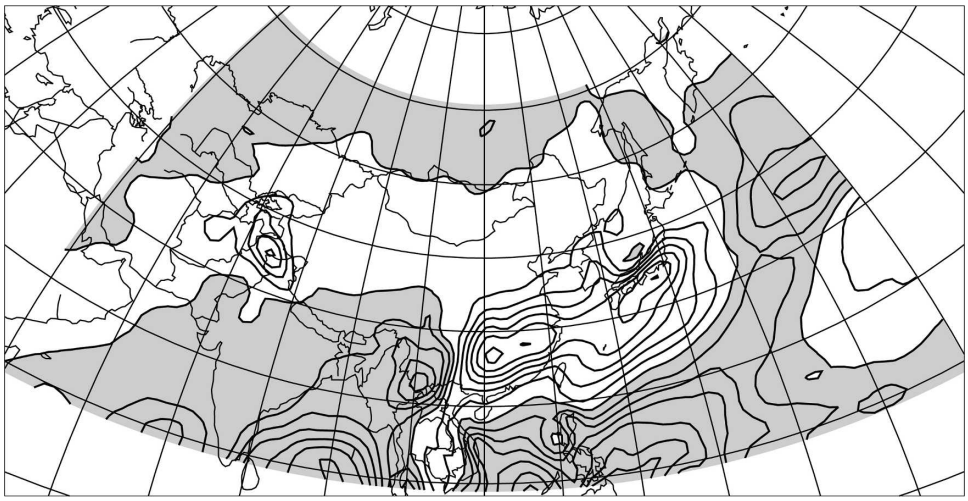

FIG. 7. Covariance $C(T_2, P|\tau)$ of T_2 with precipitation P (mm day^{-1}) in winter at $\tau = 2$ days. The contour interval is 0.2; a 9-point smoother has been applied.

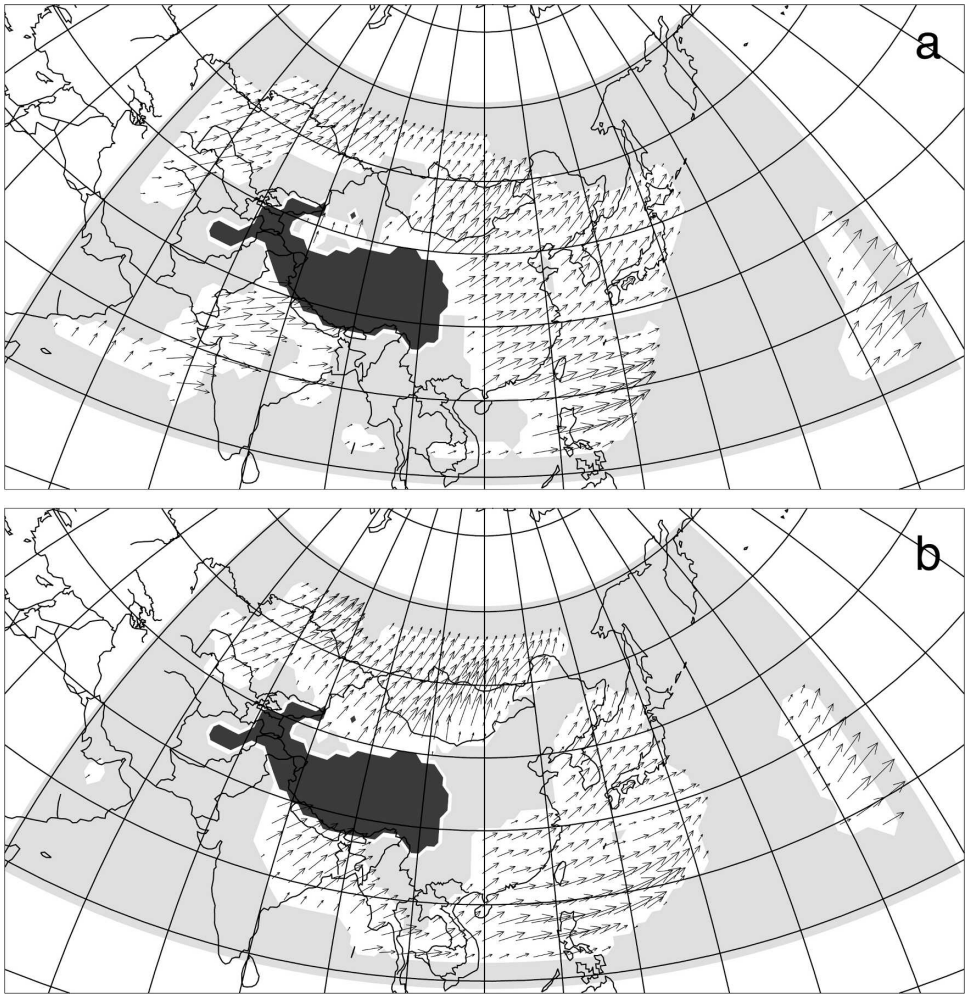

FIG. 8. Vectors $\mathbf{I} = (\alpha, \beta)$ for potential temperature covariances $C(T_2, \theta|\tau)$ in winter at (a) $\tau = -3$ days and $z = 2500$ m and at (b) $\tau = -1$ day and $z = 2500$ m. The number of grid points in the averaging domain Q for the evaluation of $\mathbf{I}$ is $M = 9 \times 9$; dark: topography; gray: (2.6) not satisfied; maximum vector length is 2.8.

generally less precipitation than normal in the southern part of the domain and more in the center. The pattern correlation of the rainfall with the observed vertical mean tendency of the temperature in that vertical column where the precipitation occurs, is negative for most lags. In particular, the strong positive precipitation anomalies out in the Pacific for $\tau \geq 2$ days occur during a phase where temperatures decay. The cooling due to upward motion at the slopes is larger than the latent heating there.

The key dynamical problem emerging from this torque event is the formation of the warm low in the lee together with that of the deep anticyclone near Japan. Theories of topographic instability (Charney and DeVore 1979; Jin and Ghil 1990) predict the growth of a low in the lee for a negative axial torque event as presented here. However, this theory requires a decrease of the area-averaged zonal flow component that has to accomplish the anomalous advection of the stationary wave pattern mentioned above. The changes of the mean zonal wind are of the order of 0.1 m s^{-1} over a few days during the torque event. They are without dynamical significance. The basic mechanism of topographic instability does not operate in this case (see also Egger and Hoinka 2008). As stated above, the torque events found here bear little resemblance to those of downstream development discussed by Chang and Yu (1999), Hakim (2003), and Chang (2005).

The orographically "enforced" vertical motion at the slopes can be assessed on the basis of Fig. 5. There is ascent and cooling all along the western slopes. Of

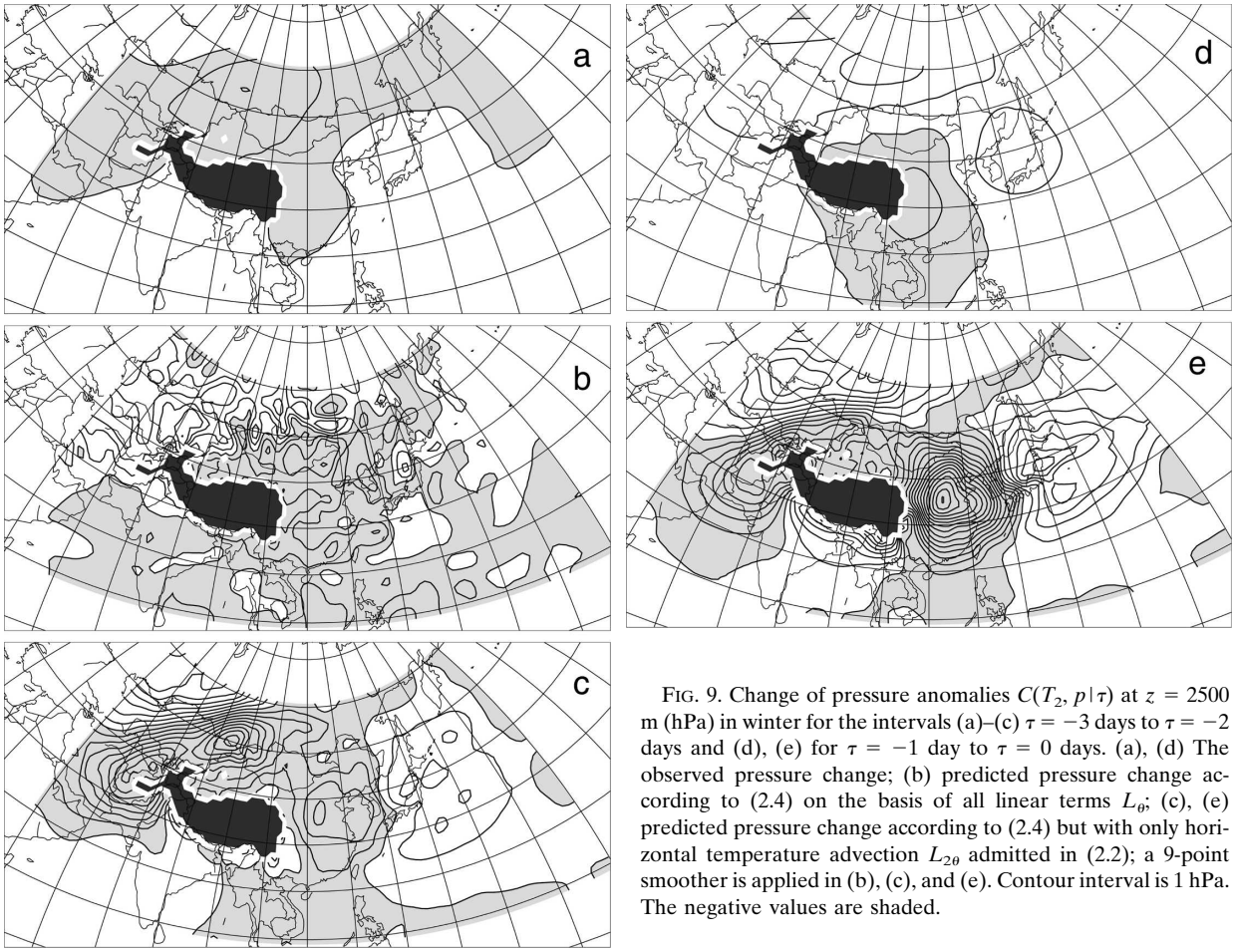

FIG. 9. Change of pressure anomalies $C(T_2, p|\tau)$ at $z = 2500$ m (hPa) in winter for the intervals (a)–(c) $\tau = -3$ days to $\tau = -2$ days and (d), (e) for $\tau = -1$ day to $\tau = 0$ days. (a), (d) The observed pressure change; (b) predicted pressure change according to (2.4) on the basis of all linear terms L_θ; (c), (e) predicted pressure change according to (2.4) but with only horizontal temperature advection $L_{2\theta}$ admitted in (2.2); a 9-point smoother is applied in (b), (c), and (e). Contour interval is 1 hPa. The negative values are shaded.

course, an inspection of the observed vertical motions at the lowest level above the topography leads to the same conclusions. There is also mainly ascent at the slope in the east and descent in the "dry" area above Burma. It follows, that the warming at the eastern slope is not supported by descent as suggested by baroclinic wave theories.

Attempts to explain observed pressure changes via (2.4) will be made for $z_o = 2500$ m. This level is below the height of the TP and above the boundary layer. We select the pressure changes from lag $\tau = -3$ days to $\tau = -2$ days as a situation of early development when the southward extension of the low is beginning to form and the corresponding change from $\tau = -1$ day to $\tau = 0$ as the moment of maximum of lee trough deepening and Japan high intensification. The related vectors $\mathbf{l} = (\alpha, \beta)$ are displayed in Fig. 8. Vectors close to the topography are somewhat questionable because the averaging domain there is smaller than, say, over the Pacific. No vectors are given at grid points where (2.6) is not satisfied. At $\tau = -3$ days (Fig. 8a), linearity is ascertained northeast and east of the TP, but not in the central Pacific. Two days later (Fig. 8b), the linear tendencies are almost perfect north of the TP but, unfortunately, not in the lee. Nevertheless, Fig. 8 suggests that the linear terms help to explain the development near the TP. We proceed, therefore, to apply (2.4). The result for $z_o = 2500$ m and a vanishing pressure covariance at the top level is displayed in Fig. 9 for comparison with the observed pressure change for the lag intervals chosen above. The observations at $\tau = -3$ days indicate pressure fall in the lee and also in the northern low. Pressure rises over Japan (Fig. 9a). Two days later (Fig. 9d), the pressure changes are more intense in the lee and also near Japan. The weakening of the trough north of the TP is clearly visible. The pressure change calculated on the basis of (2.4) indicates that pressure falls north and east of the TP, that patches of pressure rise in the east, and there are massive pressure increases in the northwest (Fig. 9b). The pressure fall in the lee is too strong as is the pressure rise northwest of the TP. It is mainly the vertical velocity that

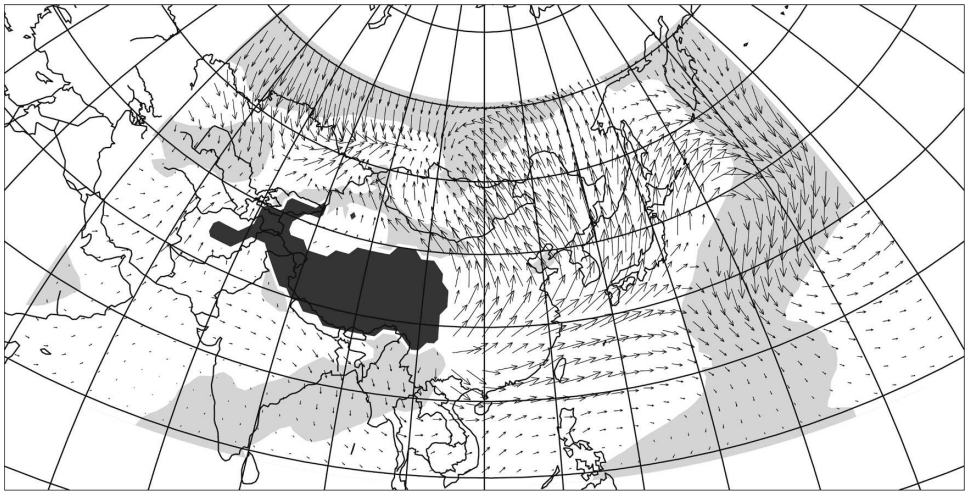

FIG. 10. Horizontal covariance vectors $C[T_2, (\mathbf{v}_2'\theta')|\tau]$ (m K s^{-1}) at $z = 2500$ m and $\tau = 2$ days; maximum vector length is 6.5 m K s^{-1}.

generates the pronounced noisiness in Fig. 9b as can be seen from Fig. 9c where only the contribution of horizontal advection to the tendency is admitted. The pressure fall in the lee and the rise over Japan are reproduced but the amplitudes are too large. It is obvious from the intercomparison that vertical motion acts as a damping factor in the lee and in the Pacific. On the other hand, the impact of vertical motion suppresses the deepening of the trough in the northwest of the TP. Its omission leads to an extreme overestimation of the pressure rise there. Guided by Fig. 9 we conclude that the pressure fall in the lee and the intensification of the Japan high is due to horizontal advection while vertical motion damps the development as is typical of baroclinic motion. This damping effect is particularly pronounced northwest of the TP. Vertical motion would have to enhance the perturbations near the slopes of the TP according to baroclinic wave theories. The vertical integration of (2.4) is carried out for $z_o = 2500$ m in Fig. 9. Instead, we are also able to look just at the impact of upper levels by excluding, for example, the levels 2500 m $\leq z \leq$ 5500 m from the vertical integration. The resulting pattern for $L_{2\theta}$ only is fairly similar to Fig. 9c. In particular, the pressure fall northwest of the TP is hardly affected. In the lee, amplitudes are about one-third of those in Fig. 9c. It is the same with the Japan high. It follows that processes at levels above the TP contribute to the development in the lee. They are, however, not the key factors there. Altogether we may state that the linear calculations provide a useful qualitative estimate but there is little quantitative guidance. Two days later, the tendency with complete L_θ included is again quite noisy (not shown). The pressure change induced by horizontal advection (Fig. 9e) is at least qualitatively correct in the lee and also with respect to the Japan high. However, the impact of vertical motion appears to dominate northwest of the TP where horizontal advection generates the pressure fall in contrast to the observations. The induced pressure change due to levels above the TP is almost identical to that in Fig. 9e except for the Japan high where amplitudes are smaller. This suggests that the southward protrusion of the low pressure regime along the slope is mainly induced by upper-level processes during its mature stage.

Thus, Fig. 9 leads to the hypothesis that the pressure fall in the lee is mainly due to warm-air advection from the south ahead of the upper-level trough. The growth of the Japan high is also mainly due to advection of cold air aloft related to the high's westward tilt with height. As in EH06, the triple terms have a rich spatial structure and vary strongly with lag. We show in Fig. 10 the horizontal flux covariance $C[T_2, (\mathbf{v}_2'\theta')|\tau]$ at $\tau = 2$ days when these fluxes are strong. It is seen that the fluxes at that time are directed mainly opposite to what one might expect. For example, there is anticyclonic flux around the "Japan high," which drifts eastward at that moment. A naive guess would have been to assume that the northerlies east of the high transport anomalously cool air so that the fluxes would have to be directed northward. However, the same result obtains for negative torques so that these contributions drop out in the covariance calculations. Thus, Fig. 10 tells us that the Japan high ($T_2 > 0$) has weaker fluxes than the corresponding Japan low for $T_2 < 0$.

b. *Equatorial torque T_1*

As indicated by Fig. 3, T_1 torque events tend to precede the T_2 events by about 1 day. They describe the

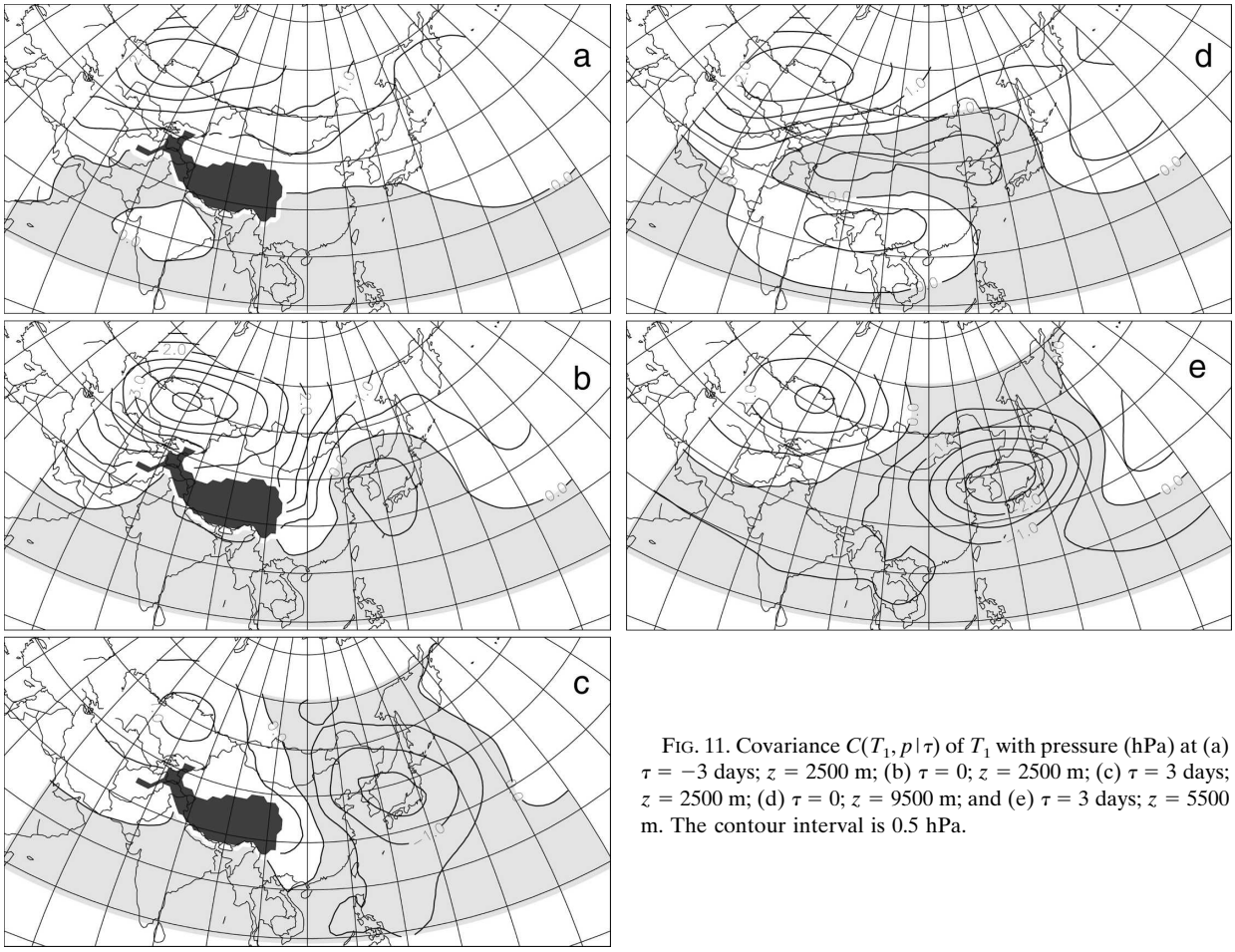

FIG. 11. Covariance $C(T_1, p \mid \tau)$ of T_1 with pressure (hPa) at (a) $\tau = -3$ days; $z = 2500$ m; (b) $\tau = 0$; $z = 2500$ m; (c) $\tau = 3$ days; $z = 2500$ m; (d) $\tau = 0$; $z = 9500$ m; and (e) $\tau = 3$ days; $z = 5500$ m. The contour interval is 0.5 hPa.

buildup of pressure anomalies at the northern edge of the TP and the following southward extension at the eastern slope. Indeed, a high pressure cell is found northeast of the TP at $\tau = -5$ days (not shown), which approaches the TP slowly during the following days. At $\tau = -3$ days (Fig. 11a), anomalously high pressure is found everywhere north of the TP but the pressure maximum is still located northwest of the TP. There are hardly any pressure anomalies at the lee slope. Southward protrusion begins at $\tau = -2$ days and a broad tongue of high pressure extends along the lee slope at $\tau = 0$ (Fig. 11b). A low emerges near Japan. The similarity to Fig. 4b is obvious. The further development of the T_1 events departs somewhat from the course of the T_2 events because the Japan low extends now toward the northwest (Fig. 11c). Compo et al. (1999) related surface pressure perturbations at leeside points to winds and pressure at various levels and found patterns quite similar to ours but for lags shifted backward by 1–2 days. The leeside protrusion appears to be more shallow than in the T_2 series. For example, there is hardly any indication of a southward-protruding high pressure tongue above the lee slope at $z = 5500$ m and $\tau = 3$ days (Fig. 11e). The pressure field at $z = 9500$ m exhibits a few special features not seen at the lower levels. In particular, a high is growing above India and the southern TP with peak intensity at $\tau = -1$ day, which is still clearly visible in Fig. 11d ($\tau = 0$). Moreover, that the Japan low is linked to a low pressure system above the TP that is first seen at $\tau = -3$ days west of the TP. Low pressure prevails above the plateau till the end of this period. The Japan low becomes weaker but does not move eastward at this height. The winds at $z = 2500$ m begin to blow southward over the China Sea at $\tau \sim -1$ day to reach maximum speeds of 4 m s^{-1} at $\tau = 2$. The flow pattern is, however, too similar to that in Fig. 5 to be presented. Given the overall similarity of T_1 and T_2 cases there is no need to display the temperature anomalies where cool air is filling the western Pacific much the same (but of opposite sign) as in Fig. 6.

The vertical motion near the lee slope shows an in-

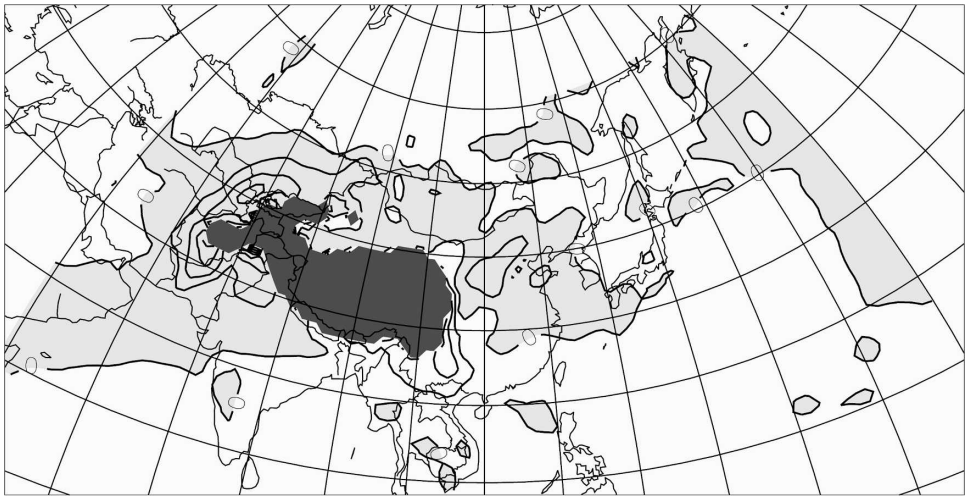

FIG. 12. Vertical motion covariance $C(T_1\ w|\tau)$ (m m s^{-1}) at $z = 2500$ m and $\tau = 0$. The contour interval is 0.2 m m s^{-1}.

teresting feature barely resolved by the analysis (Fig. 12). There is upward motion in a narrow stripe near the lee slope related to the southward protrusion of cool air. In this case, then, upward motion contributes to the cooling. This effect is, however, restricted to this narrow domain. Otherwise, there is descent almost all around the TP.

Rainfall is below normal at the southwestern slopes at all lags whereas the precipitation maximum forms at the end of the cold air protrusion in the less. At $\tau = 2$ days, the southern part of the Japan low has less rainfall than normal (Fig. 13).

The linearity tests give more positive results in this case at least for the leeside region where the linearity criterion (2.6) is satisfied for $-4 \leq \tau \leq -1$ day (not shown). Linear forecasts are fairly useless in the lee and the Pacific for $\tau > 0$. The actual computation on the basis of (2.4) show, that the contribution by horizontal temperature advection $L_{2\theta}$ gives at least a qualitatively correct answers for $\tau \leq 0$. We show in Fig. 14 the actual pressure change from $\tau = -1$ day to $\tau = 0$ as well as that given by horizontal advection. The observations indicate a continuing pressure rise north and northeast of the TP. Although the linear advection severely overestimates the amplitudes nearby all the basis features of the observations are represented in the linear calculation. The predicted pressure rise west of the TP is not realistic. The contribution by the levels above the TP is

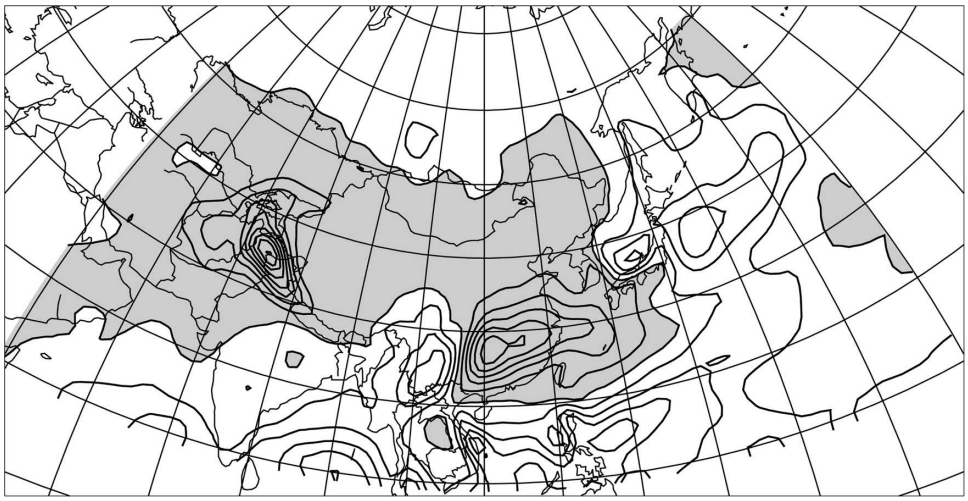

FIG. 13. Rainfall covariance of $C(T_1, P|\tau)$ (mm day^{-1}) at $\tau = 2$ days in winter. The contour interval is 0.2 mm day^{-1}.

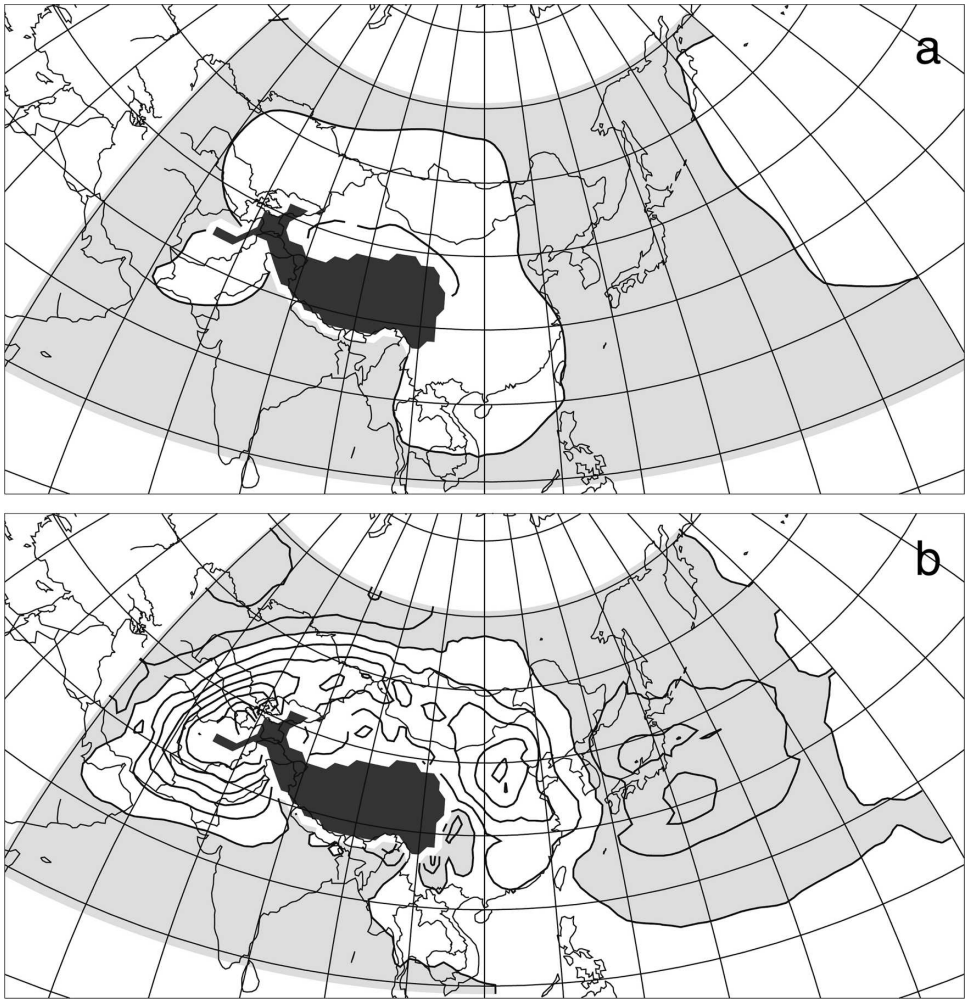

FIG. 14. Changes of pressure anomalies $C(T_1, p|\tau)$ (hPa) at $z = 2500$ m for the interval (a) -1 day $\leq \tau \leq 0$ as observed and (b) as obtained from (2.4) but with only $L_{2\theta}$ admitted. The contour interval is 1.0 hPa; a 9-point smoother has been applied in (b). Negative values are shaded.

quite strong in this case. The predicted pressure changes for the Japan low and for the high northeast of the TP are almost identical to those in Fig. 14b and only slightly smaller in the lee.

4. Conclusions and discussion

The interaction of baroclinic waves with the TP in winter has been investigated by choosing mountain torques as indicators. It turned out that the T_1 events describe the buildup of pressure anomalies at the northern flank of the TP and also capture the following southward extension along the lee slope. The T_2 events represent essentially the same phenomena but the torque T_2 peaks 1–2 days later than T_1. Thus, the T_2 events describe the motion along the slope and the following decay of the anomalies in the Pacific domain. The emergence of a circulation and pressure center near Japan is captured in both cases (Chan and Li 2004; Compo et al. 1999). On the other hand, wave motion on the southern side of the TP eludes the torque analysis.

A novel technique has been introduced in order to evaluate the eventual merits of linear explanations. Given all linear terms of the statistical potential temperature equations, a 1-day forecast for the pressure change can be made. Although these calculations turned out to be qualitatively useful, there are also substantial problems, in particular, because of the noisiness of the vertical motion fields. We are not able to decide if the low quality of the forecasts is due to the omission of the forcing and the turbulent terms or due to data problems with linear terms.

It is for the first time that precipitation maps have been presented. Rainfall anomalies at the TP are

mostly positive (negative) for upslope (downslope) flows.

Of course, cold surges are part of the ensemble of flows described by the torque analysis (Chan and Li 2004; Wu and Chan 1997). A typical cold surge events exerts a positive (negative) torque T_1 (T_2). However, also pointed out by Compo et al. (1999; their Fig. 9) there are about as many southward-moving warm air events as there are cold ones. This agrees with our findings. Compo et al. (1999) invoke the theory of shelf waves to explain this result. However, the rapid eastward extension of the temperature anomalies as depicted in Fig. 6 makes it unlikely that these broad anomalies are tied to shelf waves that would be confined to the extremely steep slope of the TP. What would be needed is a theory of baroclinic disturbances moving along meridionally oriented walls.

Baroclinic wave theories predict upward (downward) motion for cold (warm) southward leeside motion at the slope. It is not possible to decide on the basis of the available data if these theories are helpful. The slope of the TP itself is so steep that quasigeostrophic theory does not apply there. On the other hand, the inducing waves with their equivalent barotropic structure are not ideal candidates for tests. Mechanisms of topographic instability are not relevant because the changes of the mean zonal wind are quite small.

The linear pressure tendency calculations clearly show that the southward protrusion of pressure and temperature anomalies in the lee involves both the impact of upper-level flow and the dynamics of low-level motion confined by steep topography in the east. These developments differ strong from those observed near the meridionally oriented barrier of Greenland (EH06) where no southward protrusion is found and a fairly well defined anticyclone is generated in the lee during positive axial torque events.

The covariance technique does not distinguish between positive and negative torque events. Extensive calculations have been made where only positive (or negative) torque cases were admitted to the analysis. The results appeared to indicate that there is no dramatic difference between events of positive and negative sign. However, there was the problem that the seasonal cycle projects onto the results because the frequency of, for example, positive torque events varies systematically during the winter season.

It is still an open question why the perturbations during a torque event grow for $\tau \to 0$ and what makes them decay later. Baroclinic conversion appears to be partly responsible for the growth. A partial answer to this question can be provided by looking at the kinetic energy K of the flows displayed, for example, in Fig. 6.

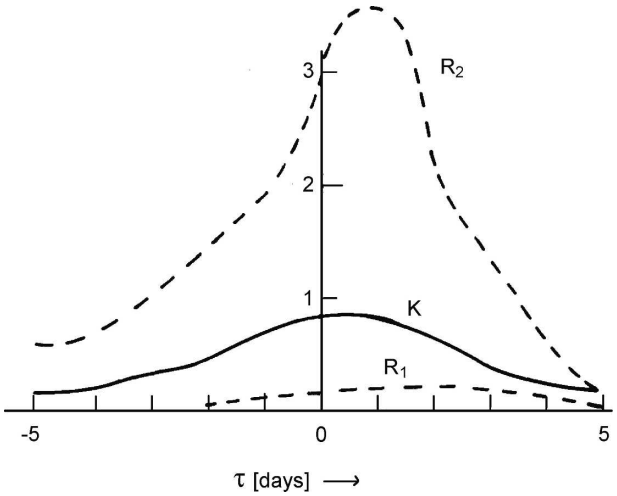

FIG. 15. Kinetic energy budget terms as a function of lagτ for the T_2 winter situation. Shown are total kinetic energy K (10^{18} J, solid), barotropic conversion term R_1(dashed), and pressure conversion term R_2 (dots) (10^{12} J s^{-1}); see text for further details.

The corresponding equations will not be written down but the result as displayed in Fig. 15 can be understood even so. The kinetic energy K grows monotonously from $\tau = -5$ days till $\tau \sim 1$ day to attain its maximum of $\sim 0.8 \times 10^{18}$ J. Such a value corresponds with a mean velocity of ~ 1.2 m s^{-1}. There is decay for $\tau > 1$ day. Inspection of the equations shows that K can be affected by conversions R_1 from the kinetic energy of the mean flow. As can be seen from Fig. 15, R_1 is positive but relatively small. The main conversion term is

$$R_2 = -\int_v C(T_2, \mathbf{v}_2|\tau) \cdot \nabla C(T_2, p|\tau)\, dV, \qquad (4.1)$$

which peaks at $\tau \sim 1$ day. This term describes conversions from the available potential energy and also those due to interactions with the atmosphere outside the analysis domain. It is large enough to approximately explain the observed increase of K so that a conventional picture of baroclinic growth appears to emerge. However, the decay of K in Fig. 15 cannot be due to R_2 because R_2 is positive and important at all lags. There is a further conversion term involving triple correlations which has not been evaluated. We speculate, that the decay of the kinetic energy K in Fig. 15 is at least partly due to this turbulence term. Surface friction does not stop the growth for $\tau < 0$ and should be not much more important for $\tau > 0$ so that the decay of the perturbations must reflect the impact of triple terms similar to what has been found near Greenland (EH06). Such conclusions must be seen with caution because of the noisiness of the tendency calculations as presented in

Fig. 9. The evaluation of energy budgets or similar calculations is highly uncertain under such circumstances. These limitations reflect sampling problems, finite difference errors in the calculation of gradients and divergences, and, of course, inaccuracies of the analyses.

Altogether, it is hoped that our results stimulate further theoretical work on the interaction of baroclinic wave systems with steep topography.

Acknowledgments. We are grateful to both referees for their detailed and constructive criticism.

APPENDIX

Torque Evaluation

The Eurasian mountain complex extends from China to the Atlantic Ocean so that a calculation of torques for this huge chain of mountains as in Weickmann (2003) includes even the pressure distribution in the Alpine region. Although the analysis of Weickmann (2003) suggests that the TP plays a key role for the Eurasian torque (see also Iskenderian and Salstein 1998), we prefer to calculate regional "torques" by modifying the topography. The corresponding procedure is illustrated in Fig. 2. The ERA-40 topography in Fig. 2a is modified (Fig. 2b) by setting the terrain height to $z = 500$ m everywhere outside the TP's 1500-m contour. Linear interpolation connects the TP's 1500-m contour with the surrounding 500-m plain. This way the block of the TP stands out almost unaltered but all contributions by terrain outside this limiting contour are discarded. It is obvious from Fig. 2b that the imposed modifications are small. The torques T_{oi} for the TP are calculated on the basis of the available surface pressure fields. Hydrostatic pressure reduction is applied in the belt with interpolated heights $500 \leq h \leq 1500$ m. Wu et al. (2005) reported on problems with the National Centers for Environmental Prediction–National Center for Atmospheric Research surface pressure analysis over the TP. No corresponding features are found in the ERA-40 data.

REFERENCES

Academia Sinica, 1958: On the general circulation over Eastern Asia (II). *Tellus,* **10,** 58–75.

Buzzi, A., A. Speranza, S. Tibaldi, and E. Tosi, 1987: A unified theory of orographic influences upon cyclogenesis. *Meteor. Atmos. Phys.,* **36,** 91–107.

Chan, J., and C. Li, 2004: The East Asia winter monsoon. *East Asian Monsoon,* World Scientific Series on Meteorology of East Asia, C.-P. Chang, Ed., Vol. 2, World Science, 54–106.

Chang, E., 2005: The impact of wave packets across Asia on Pacific cyclone development. *Mon. Wea. Rev.,* **133,** 1998–2015.

——, and D. Yu, 1999: Characteristics of wave packets in the upper troposphere. Part I: Northern Hemisphere winter. *J. Atmos. Sci.,* **56,** 1708–1728.

Charney, J., and J. DeVore, 1979: Multiple flow regimes in the atmosphere and blocking. *J. Atmos. Sci.,* **36,** 1205–1216.

Chen, S.-J., Y.-H. Kuo, P. Zhang, and Q. Bai, 1991: Synoptic climatology of cyclogenesis over East Asia, 1958–1987. *Mon. Wea. Rev.,* **119,** 1407–1418.

Compo, G., G. Kiladis, and P. Webster, 1999: The horizontal and vertical structure of East Asian winter monsoon pressure surges. *Quart. J. Roy. Meteor. Soc.,* **125,** 29–54.

Davis, Ch., 1997: A modification of baroclinic waves by the Rocky mountains. *J. Atmos. Sci.,* **54,** 848–868.

——, and M. Stoelinga, 1999: Interpretation of mountains on synoptic-scale baroclinic waves. *J. Atmos. Sci.,* **56,** 3303–3320.

Egger, J., and K.-P. Hoinka, 2006: Dynamics of atmospheric regression patterns: Regional mountain torque events. *J. Atmos. Sci.,* **63,** 1467–1482.

——, and ——, 2008: Topographic instability: Tests. *J. Atmos. Sci.,* **65,** 670–680.

Hakim, G., 2003: Developing wave packets in the North Pacific storm track. *Mon. Wea. Rev.,* **131,** 2824–2837.

Hoskins, B. J., and K. I. Hodges, 2002: New perspectives on the Northern Hemisphere winter storm tracks. *J. Atmos. Sci.,* **59,** 1041–1061.

Hsu, H.-H., and J. Wallace, 1985: Vertical structure of wintertime teleconnection patterns. *J. Atmos. Sci.,* **42,** 1693–1710.

Iskenderian, H., and D. A. Salstein, 1998: Regional sources of mountain torque variability and high-frequency fluctuations in atmospheric angular momentum. *Mon. Wea. Rev.,* **126,** 1681–1694.

Jin, F.-F., and M. Ghil, 1990: Intraseasonal oscillations in the extratropics: Hopf bifurcation and topographic instabilities. *J. Atmos. Sci.,* **47,** 3007–3022.

Joung, C. H., and M. H. Hitchman, 1982: On the role of successive downstream development in East Asia polar air outbreaks. *Mon. Wea. Rev.,* **110,** 1224–1237.

Lott, F., A. Robertson, and M. Ghil, 2004: Mountain torques and the Northern Hemisphere low-frequency variability. Part II: Regional aspects. *J. Atmos. Sci.,* **61,** 1272–1283.

Murakami, T., 1981: Orographic influence of the Tibetan Plateau on the Asiatic Winter Monsoon circulation. Part III: Short-period oscillations. *J. Meteor. Soc. Japan,* **59,** 173–200.

——, and H. Nakamura, 1983: Orographic effects on cold surges and lee-cyclogenesis as revealed by numerical experiments. Part II: Transient aspects. *J. Meteor. Soc. Japan,* **61,** 547–567.

Pierrehumbert, R., and K. Swanson, 1995: Baroclinic instability. *Annu. Rev. Fluid Mech.,* **27,** 419–467.

Ramage, C., 1971: *Monsoon Meteorology.* International Geophysical Series, Vol. 15, Academic Press, 296 pp.

Uppala, S., and Coauthors, 2005: The ERA re-analysis. *Quart. J. Roy. Meteor. Soc.,* **131,** 2961–3012.

Weickmann, K., 2003: Mountains, the global friction torque, and the circulation over the Pacific/North American region. *Mon. Wea. Rev.,* **131,** 2608–2622.

Wu, M. C., and J. C. L. Chan, 1997: Upper-level features associated with winter monsoon surges over South China. *Mon. Wea. Rev.,* **125,** 317–340.

Wu, R., J. Kinter, and B. Kirtman, 2005: Discrepancy of interdecadal changes in the Asian region among the NCEP–NCAR reanalysis, objective analyses, and observations. *J. Climate,* **18,** 3048–3067.